

Velocity Fluctuations in Fluidized Suspensions Probed by Ultrasonic Correlation Spectroscopy

M. L. Cowan,¹ J. H. Page,¹ and D. A. Weitz²

¹*Department of Physics and Astronomy, University of Manitoba, Winnipeg, Manitoba, Canada R3T 2N2*

²*Department of Physics and DEAS, Harvard University, Cambridge, Massachusetts 02138*

(Received 19 May 1999)

Velocity fluctuations in a fluidized suspension of particles are investigated using two new ultrasonic correlation spectroscopies: diffusing acoustic wave spectroscopy and dynamic sound scattering. These techniques probe both the local strain rate and rms velocity of the particles, providing important information about the spatial extent of velocity correlations. Our results demonstrate the power of these techniques to probe particle dynamics of fluidized suspensions, and suggest that the velocity correlations are essentially independent of Reynolds numbers for $Re_p < 1$.

PACS numbers: 82.70.Kj, 05.40.-a

The sedimentation of suspensions of solid particles can be counteracted by the upward flow of the surrounding fluid, thereby fluidizing the particles. Such fluidized beds are widely used in chemical reactors to bring particles and reactants into contact. They also provide a convenient means to study particle sedimentation, since the average velocity in the lab frame is zero. While the sedimentation of one or two particles can be determined exactly, hydrodynamic interactions so strongly influence particle motion that a detailed understanding of the sedimentation of many particles has remained elusive. Predictions vary widely; for example, at low particle Reynolds number $Re_p = 2a\rho_f V_0/\eta$, where viscous effects dominate inertial ones, the particle velocity fluctuations have been predicted both to diverge with system size [1] and to decay to zero due to hydrodynamic screening [2]. This startling prediction of a divergence was also supported by large-scale computer simulations [3]. Here ρ_f and η are the fluid density and viscosity, respectively, a is the particle radius, and $V_0 = \frac{2}{9}(\rho_p - \rho_f)a^2g/\eta$ is the Stokes velocity. Recent experiments [4] have clarified the behavior in this creeping flow limit. For $Re_p \sim 10^{-4}$ and for low particle volume fractions $10^{-4} < \phi < 0.1$, the velocity fluctuations were found to be correlated over a surprisingly large, ϕ -dependent length scale ξ . While the competition of ξ with system size helps rationalize some apparently contradictory observations [4], the underlying origin of this new length scale has not been established, although several explanations have been proposed [5–7]. Moreover, the behavior of the velocity correlations when Re_p is increased has not been studied experimentally, despite interesting theoretical predictions at $Re_p \sim 1$ [8]. This question is of particular interest, both because most technologically useful fluidized beds are operated at much higher Re_p and because many of the theories that account for the behavior are expansions about low Re_p , making measurements at higher Re_p a critical test to set the limits of their validity.

In this Letter, we describe two new ultrasonic correlation spectroscopies which allow us to directly probe velocity fluctuations and flow in fluidized beds at much higher Re_p

and ϕ . These spectroscopies build on the success of analogous light scattering techniques [9–11], but because the sound wavelengths are orders of magnitude larger, the ultrasonic spectroscopies probe length scales commensurate with the larger particles required for higher Re_p . The first technique, diffusing acoustic wave spectroscopy (DAWS), uses multiply scattered ultrasound to measure the variance of the relative velocity fluctuations and the local strain rate at extremely short length scales, comparable to the interparticle separations. In addition, DAWS is a unique method to investigate the length-scale dependence of the relative velocity fluctuations and hence to probe spatial correlations in the velocities. The second technique, dynamic sound scattering (DSS), uses singly scattered ultrasound to measure particle motion and determines both the mean square velocity and the dynamic correlation length of the velocity fluctuations. Together, these techniques also allow us to estimate the instantaneous velocity correlation length ξ . Most of our measurements were performed at $Re \sim 0.3$, low enough to avoid turbulence, but still orders of magnitude larger than the creeping flow measurements. Comparison with measurements at $Re_p = 0.007$ shows that the magnitude and length scale of the normalized velocity fluctuations do not vary significantly with Re_p over this range, suggesting that they are essentially independent of Reynolds number for $Re_p < O(1)$.

The fluidized bed used in our experiments contained monodisperse glass beads of radius $a = 0.438 \pm 0.012$ mm in a mixture of glycerol and water. Since the Peclet number $Pe \sim 10^{11}$, the particle motion is non-Brownian. Two different glycerol concentrations were used to vary Re_p . The bed was rectangular in shape, with cross section 120×200 mm² and a thickness L of either 7.76 or 12.2 mm. Uniform fluid injection at the bottom of the bed was ensured by careful design and testing of the distributor, which consisted of a section of closely packed glass beads held rigidly in place with fine nylon mesh (cf. [12]). By adjusting the fluid flow rate to equal the sedimentation velocity V_{sed} , the volume fraction ϕ of glass beads was varied between 0.2 and 0.5.

To probe the local velocity fluctuations of the particles, we have developed diffusing acoustic wave spectroscopy, which determines the relative particle motion from the autocorrelation function $g_1(\tau)$ of the temporal fluctuations of multiply scattered ultrasonic waves. This technique, which is analogous to the optical technique of diffusing wave spectroscopy (DWS) [10,11], uses the diffusion approximation to model propagation of multiply scattered sound through the suspension [13,14]. We used a transmission geometry, with a plane wave pulse incident on the cross section of the sample, and we detected the transmitted field in a single near-field speckle using a miniature hydrophone [13,14]. The acoustic field transmitted through the fluidized bed was measured at a fixed sampling time after a short input pulse was incident on the sample, enabling the temporal variation of the field to be measured for multiple scattering paths of length s . The decay of $g_1(\tau)$ is determined by the total phase change of diffusing sound $\Delta\phi^{(n)}(\tau)$ for $n = s/l^*$ sequential scatterings from the moving particles, where l^* is the transport mean free path. When the motion of the particles is highly correlated over length scales comparable to l^* , $\Delta\phi^{(n)}(\tau) = \sum_i^n \{k_i \cdot [\Delta\vec{r}_{i+1}(\tau) - \Delta\vec{r}_i(\tau)]\}$, where k_i is the wave vector of the wave scattered from the i th to the $(i+1)$ th particle, and $\Delta\vec{r}_{rel,i}(\tau) = \Delta\vec{r}_{i+1}(\tau) - \Delta\vec{r}_i(\tau)$ is their relative displacement. The field correlation function for pulsed DAWS then becomes [15] $g_1(\tau) = \langle e^{-i\Delta\phi^{(n)}(\tau)} \rangle \approx \exp[-(s/l^*)k^2\langle\Delta r_{rel}^2(\tau)\rangle/6]$, where $\langle\Delta r_{rel}^2(\tau)\rangle$ is the mean square displacement (msd) of the particles *relative* to their neighbors a distance l^* away and $\langle \rangle$ denotes ensemble average. This expression for $g_1(\tau)$ reduces to the form used in DWS [10,11,16–18] when the motion of the scatterers is uncorrelated on length scales $\sim l^*$, since in this case $\langle\Delta r_{rel}^2(\tau)\rangle$ is twice the single-particle msd $\langle\Delta r^2(\tau)\rangle$. In $g_1(\tau)$, $\langle\Delta r_{rel}^2(\tau)\rangle$ does not include pure rotational contributions to the relative motion, since DAWS is sensitive only to the component of $\langle\Delta r_{rel}^2(\tau)\rangle$ parallel to the scattering wave vector between adjacent scatterings. We determine s , l^* , and k from independent measurements of ballistic and diffusive sound propagation [13,14,19,20] through the suspensions, enabling the temporal evolution of $\langle\Delta r_{rel}^2(\tau)\rangle$ to be determined by inverting $g_1(\tau)$. At frequencies f above 1 MHz, the scattering is so strong that l^* is essentially equal to the nearest neighbor separation of the beads; thus these measurements probe the relative motion of adjacent beads in the suspension, providing hitherto unavailable information about the flow behavior in fluidized beds.

Typical results of our DAWS measurements at $f = 2.3$ MHz and $Re_p = 0.32$ are shown by the solid symbols in Fig. 1. At early times, $\langle\Delta r_{rel}^2(\tau)\rangle \sim \tau^2$, indicating that the particles initially move in ballistic trajectories and providing a measure of the variance in the relative velocities of the particles, $\langle\Delta r_{rel}^2(\tau)\rangle = \langle\Delta V_{rel}^2\rangle\tau^2$. At later times, however, $\langle\Delta r_{rel}^2(\tau)\rangle$ crosses over to a weaker time dependence reflecting the change in particle trajectories due to inter-

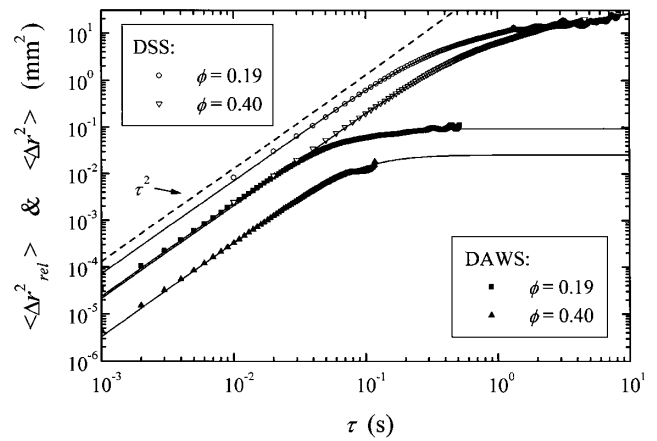


FIG. 1. Relative and absolute mean square displacements of fluidized particles at $Re \sim 0.3$ measured with DAWS (solid symbols) and DSS (open symbols). The solid curves are fits to the empirical crossover function discussed in the text.

actions with neighboring particles. We use the purely empirical relation $\langle\Delta r_{rel}^2(\tau)\rangle = \langle\Delta V_{rel}^2\rangle\tau^2/[1 + (\tau/\tau_\Delta)^{2-m}]$ to parametrize this behavior and to determine the local crossover time τ_Δ . Fits of this function to the data with $m = 0$, shown by the solid curves in Fig. 1, give an excellent description of the observed behavior and provide a quantitative measure of both $\langle\Delta V_{rel}^2\rangle$ and τ_Δ .

Because l^* becomes strongly frequency dependent below $f = 1$ MHz, we can vary the length scale over which the relative velocity fluctuations are probed by repeating these measurements at lower frequencies. Typical results for $\phi = 0.4$ are shown in Fig. 2, where we plot the length-scale dependence of $\Delta V_{rel} = \sqrt{\langle\Delta V_{rel}^2\rangle}$ normalized by V_{sed} . We find a pronounced increase of the fluctuations with the length scale; this increase is well described by $\Delta V_{rel}/V_{sed} \sim \sqrt{l^*}$, as shown by the solid line through the data. Since ΔV_{rel} is the asymptotic value of the relative velocity fluctuations as $\tau \rightarrow 0$, these data probe the spatial velocity correlations before they decay temporally.

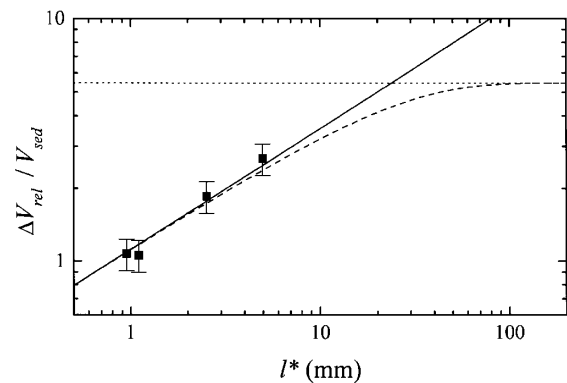


FIG. 2. Length-scale dependence of the local velocity fluctuations measured by DAWS (solid symbols), showing that $\Delta V_{rel}/V_{sed} \sim \sqrt{l^*}$ (solid line) at short length scales. The horizontal dotted line is the upper limit $\sqrt{2}\Delta V_{rms}/V_{sed}$ and the dashed line is the crossover function described in the text.

Even at the shortest length scales measured, the magnitude of ΔV_{rel} is remarkably large throughout this range of ϕ , with $\Delta V_{\text{rel}}/V_{\text{sed}} \sim 1$ at the interparticle separation; this is shown by the solid symbols in Fig. 3(a). The results depend only weakly on ϕ , first increasing and then decreasing as ϕ increases; however, there is no dependence of these local fluctuations on either L or Re_p . These measurements also allow us to determine the average local strain rate [21,22], $\Gamma = \Delta V_{\text{rel}}(l^*)/l^*$; in Fig. 3(b), we plot Γ , scaled to the mean interparticle separation and normalized by a/V_{sed} , as solid symbols. The relatively large values indicate that there are very substantial local rearrangements; moreover, there is a substantial ϕ dependence, with $\Gamma a/V_{\text{sed}} \sim \phi^{2/3}$ up to $\phi \approx 0.4$ (solid line), but decreasing at higher ϕ , indicating that the local flows become more strongly correlated.

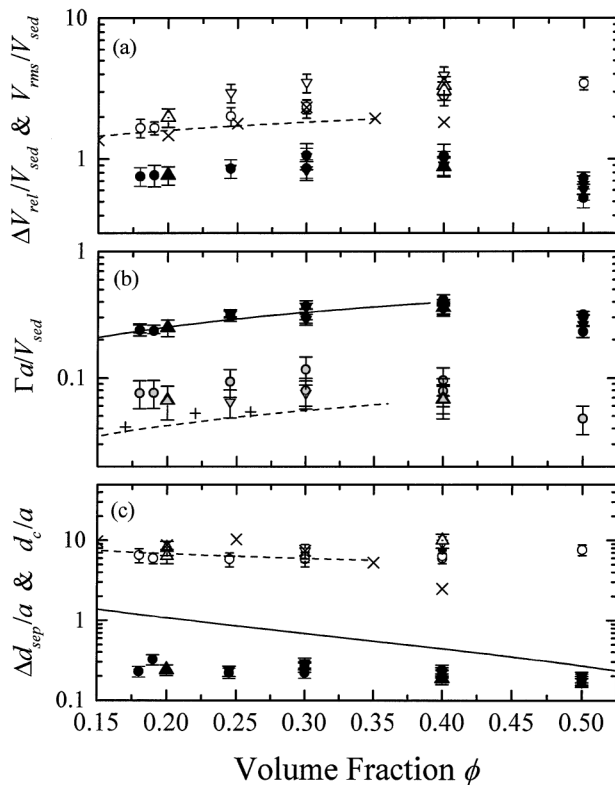


FIG. 3. (a) Local velocity fluctuations $\Delta V_{\text{rel}}/V_{\text{sed}}$ from DAWS (solid symbols) and rms velocities $V_{\text{rms}}/V_{\text{sed}}$ from DSS (open symbols). The rms velocities at $\text{Re} \sim 10^{-4}$ are shown by the crosses [23] and by the dashed line which is extrapolated from data at low ϕ [4]. (b) The normalized local strain rate from DAWS (solid symbols). Its values extrapolated to the length scale ξ (shaded symbols) are compared with results at low Re_p obtained from Refs. [4] (dashed line) and [17] (crosses). (c) Δd_{sep} (solid symbols) from DAWS compared with the mean surface-to-surface distance between the particles (solid curve), and the dynamic correlation length d_c (open symbols) from DSS compared with data at low Re_p from [23] (crosses). The dashed curve in (c) shows that $d_c \sim 4a\phi^{-1/3}$ at low ϕ . In (a), (b), and (c), the circles are data for the thin cell at $\text{Re}_p = 0.32$, while the down and up triangles are for the thick cell at $\text{Re}_p = 0.32$ and 0.007, respectively.

The DAWS data also provide a measure of a new length scale, $\Delta d_{\text{sep}} = \Delta V_{\text{rel}}\tau_{\Delta}/\sqrt{3}$, which is the average change in the separation of adjacent particles before their trajectories have been modified by interparticle interactions; we plot the ϕ dependence of $\Delta d_{\text{sep}}/a$ as solid symbols in Fig. 3(c). The largest possible value of Δd_{sep} is presumably the mean surface-to-surface distance between the beads d_{sep} , which we estimate to be approximately $2a(0.9\phi^{-1/3} - 1)$ since $d_{\text{sep}} = 0$ for close packing. We plot d_{sep} as the solid curve in Fig. 3(c); the data for Δd_{sep} are substantially lower and have a weaker ϕ dependence. This difference in the ϕ dependence suggests that there may be additional mixing on these short length scales at lower ϕ , where the flow rates are larger.

To provide a complementary probe of the fluctuations on larger length scales, we developed dynamic sound scattering, in which we use much lower frequencies, where sound is singly scattered. For single scattering, the field autocorrelation function of the temporal fluctuations is $g_1(\tau) = \exp[-\frac{1}{6}q^2\langle\Delta r^2(\tau)\rangle]$, where $q = 2k \sin(\theta/2)$ is the scattering wave vector, θ is the scattering angle, and $\langle\Delta r^2(\tau)\rangle$ is the single-particle msd. We use the same experimental geometry and determine θ from the sampling time; this is possible since the time taken for sound from the incident pulse to be singly scattered into the detector increases when θ is larger and the path length is longer. However, because of the azimuthal symmetry of our detection geometry, the measured $\langle\Delta r^2(\tau)\rangle$ is an average of the vertical and horizontal components of the particle displacements, which may differ [4]. The results for $\langle\Delta r^2(\tau)\rangle$ are shown by the open symbols in Fig. 1. The time dependence is qualitatively similar to $\langle\Delta r_{\text{rel}}^2(\tau)\rangle$, but the magnitude is substantially larger, as it is determined by the rms velocity of the beads V_{rms} . Similarly, the crossover time τ_c , which characterizes the maximum time for the particles to follow ballistic trajectories, is also larger. The crossover is more gradual for DSS than for DAWS; nevertheless, the same empirical functional form can parametrize the behavior, using $m \sim \frac{1}{2}$ and replacing $\langle\Delta V^2\rangle$ by V_{rms}^2 and τ_{Δ} by τ_c . The fits, shown in Fig. 1, are in excellent agreement with the data, providing a measure of V_{rms}^2 and τ_c .

As shown by the open symbols in Fig. 3(a), V_{rms} is roughly 2 to 3 times larger than the average fluid velocity and is substantially larger than ΔV_{rel} . The values of V_{rms} are larger for the thicker cell (down triangles), suggesting that the cell thickness may be responsible for truncating the magnitude of the velocity fluctuations [7]. In addition, our data for the thick cell show a very slight increase in V_{rms} with Re_p [down and up triangles in Fig. 3(a)]. Figure 3(a) also compares our results for V_{rms} with previous data at low Re_p [4,23], represented by the dashed curve and crosses, showing that the results obtained using these other techniques are remarkably similar, especially at low ϕ . Thus our results clearly show that Re_p is not an important control parameter in determining the magnitude of the velocity fluctuations for $\text{Re}_p < O(1)$.

Further important insight is obtained by determining the absolute distance $d_c = V_{\text{rms}}\tau_c$ traveled by the beads before their motion becomes decorrelated. As shown in Fig. 3(c), d_c is much larger than the local fluctuation distance Δd_{sep} and shows no significant variation with either L or Re_p . Up to $\phi \sim 0.3$, d_c is very similar to the average dynamic correlation length determined at lower Re_p from the temporal decay of the vertical and horizontal velocity autocorrelation functions, shown as crosses in Fig. 3(c) [23]; by contrast, at the highest ϕ , d_c does not fall off as it does in their data.

The velocity fluctuations measured with DSS determine an upper bound that cuts off the growth of ΔV_{rel} with length scale. This allows us to determine the largest length scale for velocity correlations, which must correspond to the velocity correlation length, ξ , recently observed for much lower Re_p . Since $\langle \Delta V_{\text{rel}}^2(x) \rangle = \langle [\Delta \vec{V}(x) - \Delta \vec{V}(0)]^2 \rangle = 2\langle \Delta V^2 \rangle - 2\langle \Delta \vec{V}(x) \cdot \Delta \vec{V}(0) \rangle$, and assuming that the velocity correlation function decays exponentially with distance x , we obtain $\Delta V_{\text{rel}}(x) = \sqrt{2} V_{\text{rms}} \times \sqrt{1 - e^{-x/\xi}}$. A fit to this functional form is shown by the dashed line in Fig. 2 and allows us to estimate the value of ξ . The existence of this correlation length, and its values, has not previously been determined in this range of Re_p ; at our lowest ϕ , we find that ξ is comparable to the extrapolation of the values measured at low Re_p and ϕ by Segrè *et al.* [4], but at higher ϕ , ξ can be as much as 2 to 3 times larger. These data indicate that the large-scale velocity correlations observed at low Re_p persist at higher Re_p .

Using the measured values of ξ , and the length-scale dependence of the local strain rate, we can extrapolate Γ to the largest length scales and compare it to the values of Γ measured for these length scales at low Re_p . We do this in Fig. 3(b), where our data are plotted as shaded points and are compared to values from data at $\text{Re}_p \sim 10^{-4}$, shown by the crosses [17], as well as the extrapolation of $\Gamma a / V_{\text{sed}} \approx \Delta V_{\text{rms}} / \xi \approx 0.1a\phi^{2/3}$, shown by the dashed line [4]. Our results are somewhat larger, although we do not see a significant Re_p dependence in our data. Interestingly, as shown by the solid line in Fig. 3(b), the normalized strain rate at short length scales exhibits the same $\phi^{2/3}$ dependence at low ϕ , although it is nearly an order of magnitude larger. In addition, the dynamic correlation length d_c is typically one-sixth of ξ in the range of ϕ investigated, suggesting that the velocity correlations evolve substantially in the time τ_c over which d_c is measured; thus the lifetime of the correlated regions is so short that the particles can move only a small fraction of ξ before their velocities become decorrelated.

The ultrasonic techniques described here provide a valuable new approach for investigating the behavior of fluidized suspensions over a wide range of Re_p and ϕ . Our results, showing that the velocity fluctuations are nearly independent of Re_p , at least for $\text{Re}_p < 1$, serve as an important benchmark for future theoretical work, which is required to unambiguously determine the origin of the velocity correlations.

Acknowledgment is made to NSERC, NATO, Imperial Oil Ltd., and the donors of the Petroleum Research Fund, administered by the ACS, for support of this research.

-
- [1] R. E. Caflisch and J. H. C. Luke, *Phys. Fluids* **28**, 759 (1985).
 - [2] D. L. Koch and E. S. G. Shaqfeh, *J. Fluid Mech.* **224**, 275 (1991).
 - [3] A. J. C. Ladd, *Phys. Rev. Lett.* **76**, 1392 (1996).
 - [4] P. N. Segrè, E. Herbolzheimer, and P. M. Chaikin, *Phys. Rev. Lett.* **79**, 2574 (1997).
 - [5] A. Levine, S. Ramaswamy, E. Frey, and R. Bruinsma, *Phys. Rev. Lett.* **81**, 5944 (1998).
 - [6] P. Tong and B. J. Ackerson, *Phys. Rev. E* **58**, R6931 (1998).
 - [7] M. P. Brenner, *Phys. Fluids* **11**, 754 (1999).
 - [8] D. L. Koch, *Phys. Fluids A* **5**, 1141 (1993).
 - [9] B. J. Berne and R. Pecora, *Dynamic Light Scattering* (Wiley-Interscience, New York, 1976).
 - [10] D. J. Pine, D. A. Weitz, P. M. Chaikin, and E. Herbolzheimer, *Phys. Rev. Lett.* **60**, 1134 (1988).
 - [11] G. Maret and P. E. Wolf, *Z. Phys. B* **65**, 409 (1987).
 - [12] A. K. Didwania and G. M. Homsy, *Int. J. Multiph. Flow* **7**, 563 (1981).
 - [13] J. H. Page, H. P. Schriemer, A. E. Bailey, and D. A. Weitz, *Phys. Rev. E* **52**, 3106 (1995).
 - [14] H. P. Schriemer, M. L. Cowan, J. H. Page, P. Sheng, Z. Liu, and D. A. Weitz, *Phys. Rev. Lett.* **79**, 3166 (1997).
 - [15] M. L. Cowan, I. P. Jones, J. H. Page, and D. A. Weitz (unpublished).
 - [16] A. G. Yodh, P. D. Kaplan, and D. J. Pine, *Phys. Rev. B* **42**, 4744 (1990).
 - [17] J.-Z. Xue, E. Herbolzheimer, M. A. Rutgers, W. B. Russel, and P. M. Chaikin, *Phys. Rev. Lett.* **69**, 1715 (1992).
 - [18] N. Menon and D. J. Durian, *Science* **275**, 1920 (1997).
 - [19] J. H. Page, P. Sheng, H. P. Schriemer, I. Jones, X. Jing, and D. A. Weitz, *Science* **271**, 634 (1996).
 - [20] M. L. Cowan, K. Beaty, J. H. Page, Z. Liu, and P. Sheng, *Phys. Rev. E* **58**, 6626 (1998).
 - [21] D. Bicout and R. Maynard, *Physica (Amsterdam)* **199A**, 387 (1993).
 - [22] D. Bicout and G. Maret, *Physica (Amsterdam)* **210A**, 87 (1994).
 - [23] H. Nicolai, B. Herzhaft, E. J. Hinch, L. Oger, and E. Guazzelli, *Phys. Fluids* **7**, 12 (1995).